Beyond a Pure Stochastic Treatment: Integrating Remaining Systematics into Congruency Tests

Reza Naeimaei[1] (ORCID)& Steffen Schön[1] (ORCID)

[1] Institut für Erdmessung (IfE), Leibniz Universität Hannover, Hannover, Germany
naeimaei@ife.uni-hannover.de (corresponding author), schoen@ife.uni-hannover.de

DOI: 10.3217/978-3-99161-070-0-013, CC BY 4.0

Abstract

Monitoring the deformations of both natural and man-made structures is a central task in engineering geodesy. Terrestrial laser scanning (TLS) is well-established for detecting geometric changes at the centimeter level. However, at the millimeter scale, the differences observed from one epoch to another may arise from either actual deformation or remaining systematic errors present in the processing chain. Classical congruency tests assess significance based on a purely stochastic model, which can lead to overly optimistic results when systematic effects are significant.

We propose an interval-extended 2D congruency test for planar displacement vectors. The stochastic part is treated probabilistically through a covariance matrix, while remaining systematic effects are represented as unknown-but-bounded deviations within an admissible set $\mathcal{B} \subset \mathbb{R}^2$. For each observation $\boldsymbol{d}$, the quadratic-form statistic becomes interval-valued, $[T] = [T_{\min}, T_{\max}]$, which induces a three-valued decision rule: *strict accept* (stable for all admissible biases), *reject* (deformed for all admissible biases), and an intermediate *ambiguous* region where bias and deformation are not separable. In 2D, the regions admit a transparent geometric interpretation via Minkowski sum and difference of the classical acceptance ellipse with $\mathcal{B}$.

Bias–noise separated Monte Carlo experiments quantify conditional decision probabilities as bias maps over the admissible set $\mathcal{B}$. We compare an axis-aligned error box with a generator-based zonotope to illustrate how the chosen systematic model affects the size and structure of the ambiguity region.

1 Motivation and Scope

In high-precision deformation monitoring, apparent epoch-to-epoch differences may reflect true geometric change, but they may also be induced by measurement effects such as residual registration artefacts, incidence-angle dependent effects, atmospheric variability, or surface reflectance changes. When monitoring at the millimeter level, remaining systematic effects can be of the same order as the sought signal. A purely stochastic uncertainty model may then

underestimate the risk of false decisions. Classical concepts of network-based deformation analysis and congruency testing are discussed, for example, in (Caspary and Rüeger, 1987; Heunecke et al., 2013). Early extensions that explicitly account for observation imprecision (remaining systematic error) in hypothesis testing and congruency testing are presented in (Neumann and Kutterer, 2007, 2006). Recent work on terrestrial laser scanning has developed interval-based uncertainty bounding and deterministic interval uncertainty models that separate stochastic variability from bounded systematic effects. These models provide the methodological basis for constructing plausible admissible bias sets (see references (Naeimaei and Schön, 2025a,b)). A broader perspective on dealing with uncertainty beyond purely probabilistic error models is provided in (Kutterer, 2002).

This contribution focuses on the decision step in deformation analysis: testing whether an observed displacement is compatible with zero deformation. We treat stochastic variability with the conventional covariance-based model, but represent remaining systematics as bounded sets. The resulting interval test aims to (i) avoid overconfident binary decisions, (ii) separate robust decisions from non-identifiable situations, and (iii) provide an interpretable geometry that can support diagnostics and communication of uncertainty.

2 2D Congruency Test

2.1 Measurement Model and Hypotheses

Let $\boldsymbol{d} \in \mathbb{R}^2$ denote an observed planar displacement between two epochs. We adopt the additive model

$$\boldsymbol{d} = \boldsymbol{\mu}_d + \boldsymbol{b} + \boldsymbol{e}, \qquad \boldsymbol{e} \sim \mathcal{N}(\mathbf{0}, \boldsymbol{\Sigma}_d), \tag{1}$$

where $\boldsymbol{\mu}_d$ is the true displacement, $\boldsymbol{e}$ is the stochastic component, and $\boldsymbol{b}$ represents remaining systematic effects that are unknown but bounded. The hypotheses are

$$H_0 : \boldsymbol{\mu}_d = \mathbf{0} \qquad \text{vs.} \qquad H_a : \boldsymbol{\mu}_d \neq \mathbf{0}. \tag{2}$$

2.2 Classical Congruency Test

In the nominal case ($\boldsymbol{b} = \mathbf{0}$), the quadratic form

$$T_{\text{cls}} = \boldsymbol{d}^\top \boldsymbol{\Sigma}_d^{-1} \boldsymbol{d} \tag{3}$$

is χ^2-distributed with $h = 2$ degrees of freedom under H_0. For significance level α, the critical value is $k_\alpha = \chi^2_{2,1-\alpha}$ and the classical acceptance region is the ellipse

$$\mathcal{E} = \left\{ \boldsymbol{d} : \boldsymbol{d}^\top \boldsymbol{\Sigma}_d^{-1} \boldsymbol{d} \leq k_\alpha \right\}. \tag{4}$$

The decision is binary: accept H_0 if $T_{\text{cls}} \leq k_\alpha$ and reject otherwise.

This classical formulation is standard in geodetic deformation analysis and congruency testing under Gaussian assumptions (Caspary and Rüeger, 1987; Heunecke et al., 2013).

Analytical power (classical test). Under a fixed mean displacement $\boldsymbol{m} = \boldsymbol{\mu}_d + \boldsymbol{b}$, the quadratic form T_{cls} follows a non-central χ^2 distribution with $h = 2$ degrees of freedom and non-centrality parameter

$$\lambda(\boldsymbol{b}) = \boldsymbol{m}^\top \boldsymbol{\Sigma}_d^{-1} \boldsymbol{m} = (\boldsymbol{\mu}_d + \boldsymbol{b})^\top \boldsymbol{\Sigma}_d^{-1} (\boldsymbol{\mu}_d + \boldsymbol{b}). \tag{5}$$

This yields $P(\text{reject} \mid \boldsymbol{b}) = 1 - F_{\chi^2_{2,\lambda(\boldsymbol{b})}}(k_\alpha)$ and provides a reference for Monte Carlo results.

2.3 Interval-Extended Congruency Test

To incorporate remaining systematic effects, the unknown bias vector $\boldsymbol{b}$ is constrained to a bounded set $\mathcal{B} \subset \mathbb{R}^2$. We consider two practical models:

(a) Error box. An axis-aligned box

$$\mathcal{B} = B = [-\Delta_x, \Delta_x] \times [-\Delta_y, \Delta_y]. \tag{6}$$

(b) Zonotope. A generator-based zonotope

$$\mathcal{B} = Z = \left\{ \sum_{i=1}^{p} \zeta_i \, \boldsymbol{g}^{(i)} : \zeta_i \in [-1, 1] \right\} = \{ \boldsymbol{G}\boldsymbol{\zeta} : \boldsymbol{\zeta} \in [-1, 1]^p \}, \tag{7}$$

with a generator matrix $\boldsymbol{G} = [\boldsymbol{g}^{(1)} \ \cdots \ \boldsymbol{g}^{(p)}] \in \mathbb{R}^{2\times p}$. Zonotopes can encode preferred directions of bounded deviations and dependencies between displacement components.

For a hypothetical admissible bias $\boldsymbol{b} \in \mathcal{B}$, the bias-corrected displacement is $\boldsymbol{d} - \boldsymbol{b}$ and the associated quadratic form is

$$T_{\text{ext}}(\boldsymbol{b}) = (\boldsymbol{d} - \boldsymbol{b})^\top \boldsymbol{\Sigma}_d^{-1} (\boldsymbol{d} - \boldsymbol{b}). \tag{8}$$

Because $\boldsymbol{b}$ is unknown but bounded, the statistic becomes interval-valued (Moore et al., 2009),

$$[T] = [T_{\min}, T_{\max}], \qquad T_{\min} = \min_{\boldsymbol{b}\in\mathcal{B}} T_{\text{ext}}(\boldsymbol{b}), \quad T_{\max} = \max_{\boldsymbol{b}\in\mathcal{B}} T_{\text{ext}}(\boldsymbol{b}). \tag{9}$$

Using the same critical value $k_\alpha = \chi^2_{2,1-\alpha}$ as in the classical test, the extended decision rule is:

$$\text{strict accept} \quad \Leftrightarrow \quad T_{\max} \le k_\alpha, \tag{10}$$

$$\text{reject} \quad \Leftrightarrow \quad T_{\min} \ge k_\alpha, \tag{11}$$

$$\text{ambiguous} \quad \Leftrightarrow \quad T_{\min} \le k_\alpha < T_{\max}. \tag{12}$$

Geometric interpretation. Let $\mathcal{E} = \{\boldsymbol{d} : \boldsymbol{d}^\top \boldsymbol{\Sigma}_d^{-1} \boldsymbol{d} \le k_\alpha\}$ denote the classical acceptance ellipse. The interval extension induces three decision regions that can be described using Minkowski operations (sum $\oplus$ and difference $\ominus$), summarized in Table 1. Intuitively, the inner region $\mathcal{E} \ominus \mathcal{B}$

contains displacements that remain inside $\mathcal{E}$ even after adding any admissible bias, while the outer region $\mathcal{B} \oplus \mathcal{E}$ expands $\mathcal{E}$ by all admissible biases. Displacements outside $\mathcal{B} \oplus \mathcal{E}$ cannot be explained by any admissible bias and are therefore rejected robustly. The grey zone in between corresponds to a structural identifiability limit: without additional information, deformation and admissible bias cannot be separated.

Tabelle 1: Geometric characterization of decision regions for the interval-extended congruency test.

Region	Set expression	Interpretation
Outer region	$A_{\text{ext}} = \mathcal{B} \oplus \mathcal{E}$	Outside A_{ext}, deformation is certain (reject).
Inner region	$A_{\text{in}} = \mathcal{E} \ominus \mathcal{B}$	Inside A_{in}, stability is certain (strict accept).
Grey zone	$A_{\text{amb}} = A_{\text{ext}} \setminus A_{\text{in}}$	Bias and deformation are not separable (ambiguous).

2.4 Monte Carlo Design (Bias–Noise Separation)

We estimate conditional decision probabilities by separating deterministic bias from stochastic noise. For a fixed admissible bias $\boldsymbol{b} \in \mathcal{B}$, we generate

$$\boldsymbol{d}^{(j)} = \boldsymbol{\mu}_d + \boldsymbol{b} + \boldsymbol{e}^{(j)}, \qquad \boldsymbol{e}^{(j)} \sim \mathcal{N}(\mathbf{0}, \boldsymbol{\Sigma}_d), \qquad j = 1, \ldots, N_{\text{stoch}}, \tag{13}$$

and compute empirical frequencies $\widehat{P}(\text{strict accept} \mid \boldsymbol{b})$, $\widehat{P}(\text{ambiguous} \mid \boldsymbol{b})$, and $\widehat{P}(\text{reject} \mid \boldsymbol{b})$. Repeating this for a set of biases $\{\boldsymbol{b}_k\}_{k=1}^{N_{\text{bias}}} \subset \mathcal{B}$ yields decision maps over bias space.

3 Simulation Study: Box and Zonotope Models

3.1 Error-Box Example (units in cm)

Configuration:

$$\boldsymbol{\mu}_d = \begin{bmatrix} 2 \\ 1 \end{bmatrix}, \quad \boldsymbol{\Sigma}_d = \begin{bmatrix} 0.8^2 & 0 \\ 0 & 0.5^2 \end{bmatrix}, \quad \mathcal{B} = [-\Delta_x, \Delta_x] \times [-\Delta_y, \Delta_y],\ \Delta_x = \Delta_y = 0.2, \quad \alpha = 0.05.$$

Here, $\Delta_x = \Delta_y = 0.2\,\text{cm}$ corresponds to $\pm 2\,\text{mm}$; therefore the bias maps are evaluated over $(b_x, b_y) \in [-2, 2] \times [-2, 2]$ mm. For the box case, we evaluate a regular bias grid with $n_{\text{grid}} = 200$ points per axis ($N_{\text{bias}} = n_{\text{grid}}^2$) and use $N_{\text{stoch}} = 2000$ noise realizations per bias.

Bias maps (classical vs. interval-extended). Figure 1 shows conditional decision probabilities as functions of the fixed bias $\boldsymbol{b} = (b_x, b_y)^\top \in \mathcal{B}$. Under H_a, the classical rejection probability is driven by the noncentrality parameter $\lambda(\boldsymbol{b})$; biases aligned with $\boldsymbol{\mu}_d$ increase detection probability, while opposing biases reduce it. In the interval-extended test, decision mass is redistributed among *reject*, *ambiguous*, and *strict accept*, reflecting whether the observation can be explained

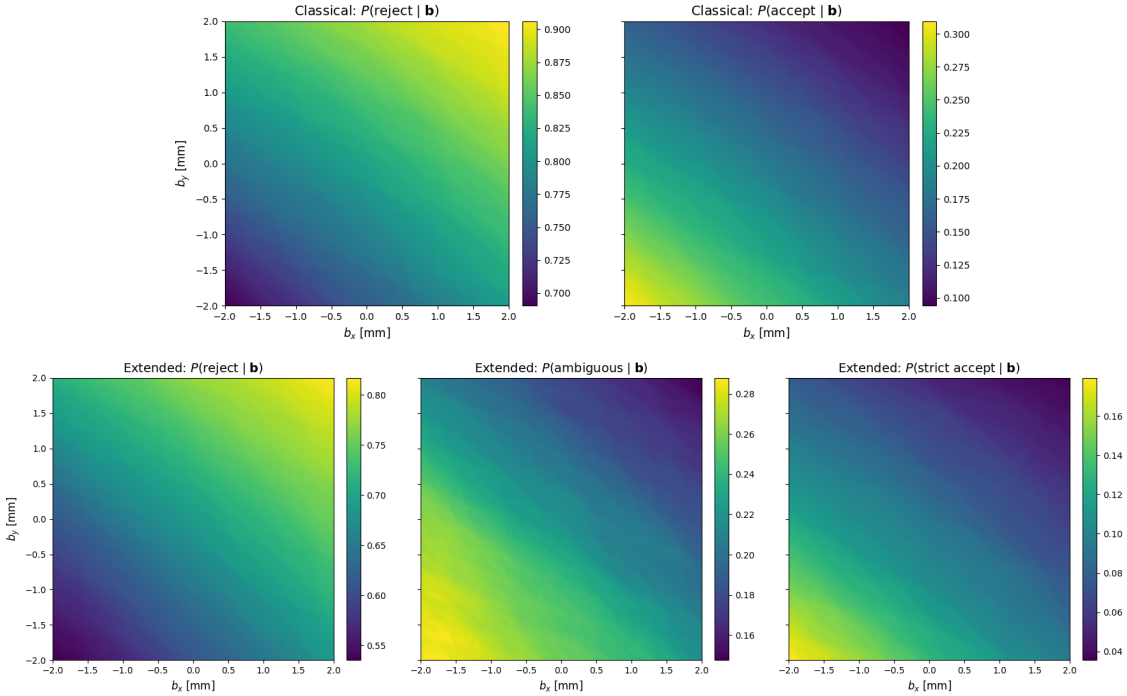

Abb. 1: Error-box case: bias maps over $\boldsymbol{b} \in [-2,2] \times [-2,2]$ mm. Top: classical maps $P_{\mathrm{cls}}(\text{reject} \mid \boldsymbol{b})$ and $P_{\mathrm{cls}}(\text{accept} \mid \boldsymbol{b})$. Bottom: extended maps $P_{\mathrm{ext}}(\text{reject} \mid \boldsymbol{b})$, $P_{\mathrm{ext}}(\text{ambiguous} \mid \boldsymbol{b})$, and $P_{\mathrm{ext}}(\text{strict accept} \mid \boldsymbol{b})$.

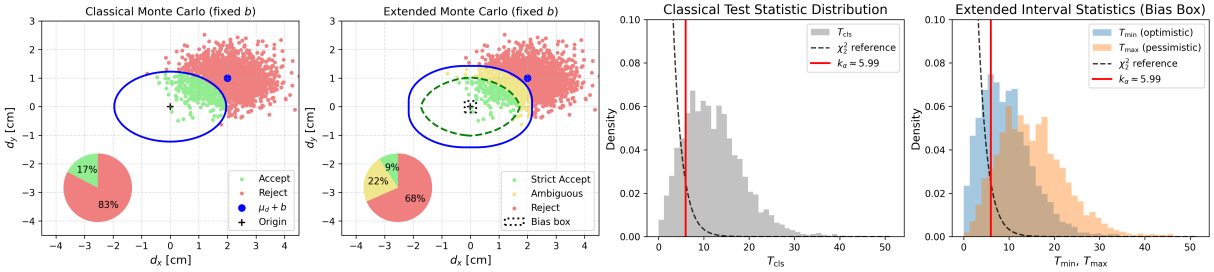

(a) $\boldsymbol{b} = \boldsymbol{b}_0 = [0,0]^\top$ mm.

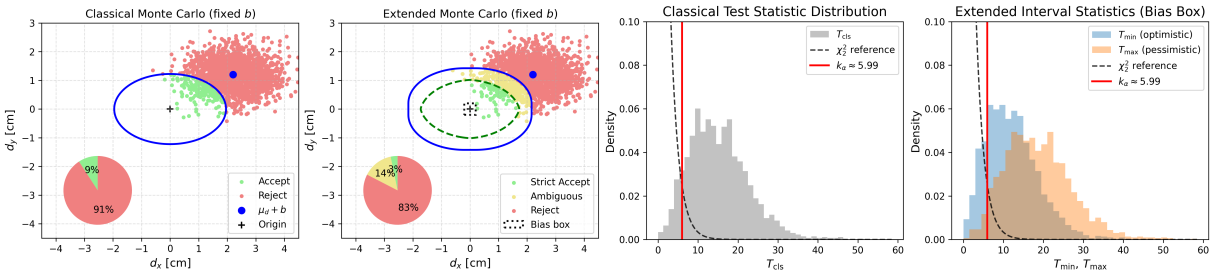

(b) $\boldsymbol{b} = \boldsymbol{b}_{\max} = [2,2]^\top$ mm.

Abb. 2: Error-box case: conditional Monte Carlo displacement samples and decisions for two fixed bias settings (centre and extreme).

by an admissible bias correction. In particular, the ambiguous probability is largest where the deterministic bias most effectively counteracts the mean displacement.

Representative conditional clouds and statistics. We illustrate two fixed settings, $\boldsymbol{b}_0 = (0,0)^\top$ mm and $\boldsymbol{b}_{\max} = (2,2)^\top$ mm. Figure 2 summarizes the corresponding conditional Monte Carlo outcomes: for each bias setting it shows the displacement cloud together with the decision regions, and the associated empirical distributions of T_{cls} as well as the interval endpoints $(T_{\min}, T_{\max})$ relative to the critical value k_α. The spread between $T_{\min}$ and $T_{\max}$ quantifies how strongly admissible bias corrections can shift the statistic from an optimistic (best-case) to a pessimistic (worst-case) interpretation.

3.2 Zonotope Example

A zonotope bias model represents remaining systematic effects with structured behavior between components. We use

$$\boldsymbol{\mu}_d = \begin{bmatrix} 2 \\ 1 \end{bmatrix}, \quad \boldsymbol{\Sigma}_d = \begin{bmatrix} 0.8^2 & 0 \\ 0 & 0.5^2 \end{bmatrix}, \quad \mathcal{B} = \{\boldsymbol{G}\boldsymbol{u} : \boldsymbol{u} \in [-1,1]^3\}, \quad \boldsymbol{G} = \begin{bmatrix} 0.2 & 0 & 0.2 \\ 0 & 0.2 & 0.2 \end{bmatrix}, \quad \alpha = 0.05.$$

Because the third generator contributes to both components, the bounding box of $\mathcal{B}$ extends to ± 4 mm in each coordinate; therefore the maps are shown over $(b_x, b_y) \in [-4,4] \times [-4,4]$ mm, with values defined only inside the admissible zonotope. For visualization, admissible biases are generated by sampling $\boldsymbol{u} \in [-1,1]^3$ and setting $\boldsymbol{b} = \boldsymbol{G}\boldsymbol{u}$. This procedure yields a dense coverage of $\mathcal{B}$, but is not strictly uniform inside the zonotope; exact uniform sampling is not required for the conditional map visualization shown here.

Bias maps (classical vs. interval-extended). Figure 3 reports conditional decision probabilities as functions of the fixed bias $\boldsymbol{b} \in \mathcal{B}$. The zonotope's preferred directions induce an anisotropic admissible bias set, which in turn changes the extent and shape of the ambiguity region compared to the axis-aligned box.

Representative conditional clouds and statistics. We again show two fixed settings, $\boldsymbol{b}_0 = (0,0)^\top$ mm and $\boldsymbol{b}_{\max} = (2,2)^\top$ mm. Figure 4 summarizes the corresponding conditional outcomes: for each bias setting, it shows the displacement cloud together with the decision regions, and the associated empirical distributions of T_{cls} and $(T_{\min}, T_{\max})$ relative to the critical value k_α.

4 Discussion and Conclusions

When remaining systematic effects are modeled as a bounded set $\mathcal{B}$, the classical quadratic-form statistic extends to an interval $[T] = [T_{\min}, T_{\max}]$. This yields a three-valued decision rule that distinguishes outcomes that are robust to *all* admissible biases (*strict accept* or *reject*) from outcomes that cannot be decided without additional information (*ambiguous*). In the 2D setting, the geometry is explicit: the classical acceptance ellipse $\mathcal{E}$ induces an inner strict-accept region $\mathcal{E} \ominus \mathcal{B}$ and an outer robust-reject boundary $\mathcal{B} \oplus \mathcal{E}$, with the grey zone between them.

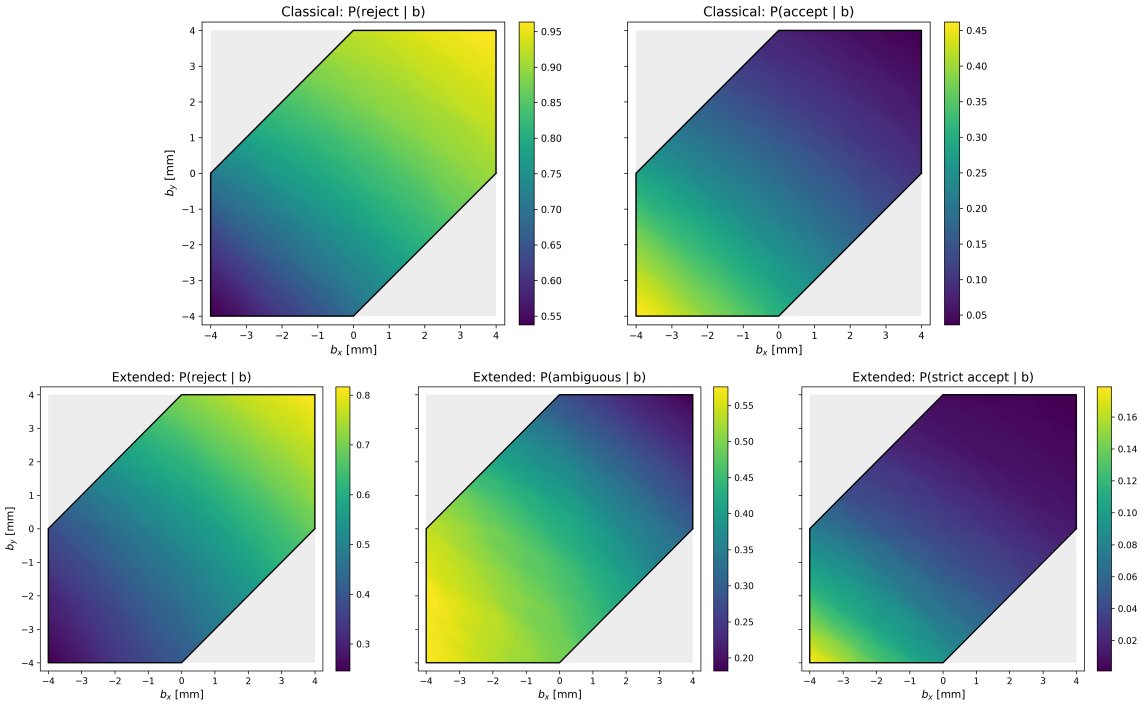

Abb. 3: Error-box case: bias maps over $\boldsymbol{b} \in [-2,2] \times [-2,2]$ mm. Top: classical maps $P_{\text{cls}}(\text{reject} \mid \boldsymbol{b})$ and $P_{\text{cls}}(\text{accept} \mid \boldsymbol{b})$. Bottom: extended maps $P_{\text{ext}}(\text{reject} \mid \boldsymbol{b})$, $P_{\text{ext}}(\text{ambiguous} \mid \boldsymbol{b})$, and $P_{\text{ext}}(\text{strict accept} \mid \boldsymbol{b})$.

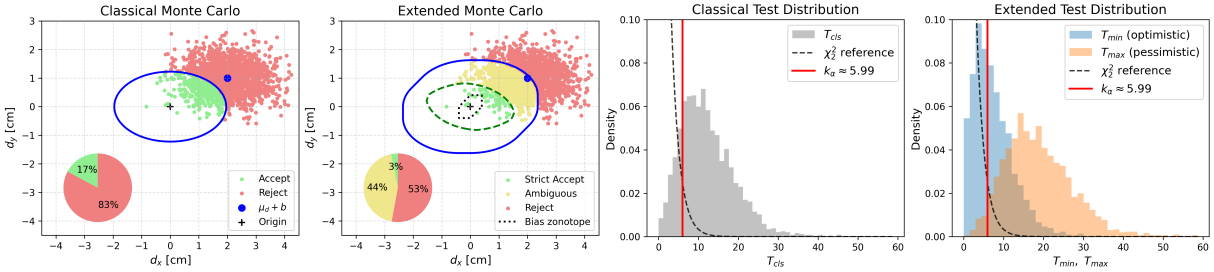

(a) $\boldsymbol{b} = \boldsymbol{b}_0 = [0,0]^\top$ mm.

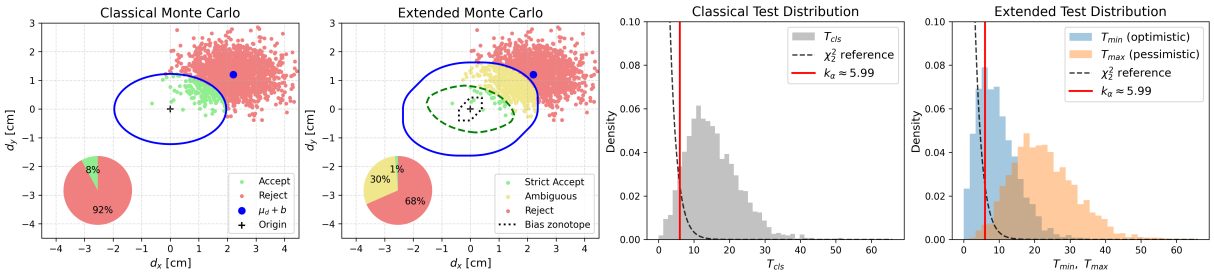

(b) $\boldsymbol{b} = \boldsymbol{b}_{\max} = [2,2]^\top$ mm.

Abb. 4: Zonotope case: conditional Monte Carlo displacement samples and decisions for two fixed bias settings (centre and extreme).

The simulations demonstrate that ignoring remaining systematics can substantially shift the binary decision probabilities of the classical test, particularly when admissible biases are aligned or anti-aligned with the displacement direction. The interval extension avoids overconfident conclusions by allocating probability mass to an interpretable ambiguity region. The size and

structure of this region depend on both the stochastic anisotropy (through $\mathbf{\Sigma}_d$) and the chosen bias model (box versus zonotope). In practice, this implies that constructing a plausible admissible set $\mathcal{B}$ is a central modeling step and should be tied to the dominant residual systematic effects of the employed sensor and processing pipeline.

Effect of set geometry and orientation. The ambiguity region is governed by the geometry of $\mathcal{B}$ relative to the stochastic acceptance ellipse. For an axis-aligned box, the Minkowski difference $\mathcal{E} \ominus \mathcal{B}$ can be interpreted as shrinking the ellipse by the box support function; hence, directions where the ellipse is narrow relative to the box are affected most. If $\mathbf{\Sigma}_d$ is not diagonal (rotated ellipse), the grey zone changes accordingly because the admissible set and ellipse are no longer aligned. Zonotopes generalize this behavior by introducing preferred directions via their generators, which can enlarge or reduce the grey zone anisotropically.

Outlook. Future work will focus on (a) deriving admissible bias sets $\mathcal{B}$ from TLS processing chains (registration, surface modeling, and incidence-angle effects), (b) exact computation of $T_{\min}$ and $T_{\max}$ via convex optimization and vertex enumeration for general polytopes, and (c) extension to higher-dimensional displacement parameters and spatially distributed tests on surfaces.

References

CASPARY, W & RÜEGER, J.M. *Concepts of Network and Deformation Analysis*. Number 11. School of Surveying, The University of New South Wales, Kensington, NSW, 1987. ISBN 0858390442.

HEUNECKE, O, KUHLMANN, H, WELSCH, W, EICHHORN, A, & NEUNER, H. *Handbuch Ingenieurgeodäsie: Auswertung geodätischer Überwachungsmessungen*. Wichmann, Berlin/Offenbach, 2., neu bearbeitete und erweiterte auflage edition, 2013.

KUTTERER, H. Zum umgang mit ungewissheit in der geodäsie: Bausteine für eine neue fehlertheorie. Reihe C 553, Deutsche Geodätische Kommission (DGK), München, 2002.

MOORE, R.E, KEARFOTT, R.B, & CLOUD, M.J. *Introduction to Interval Analysis*. SIAM, Philadelphia, PA, 2009.

NAEIMAEI, R & SCHÖN, S. Interval-based uncertainty bounding for terrestrial laser scanning observations. *ISPRS Annals of the Photogrammetry, Remote Sensing and Spatial Information Sciences*, X-G-2025:599–606, 2025a. doi: 10.5194/isprs-annals-X-G-2025-599-2025. ISPRS Geospatial Week 2025.

NAEIMAEI, R & SCHÖN, S. Deterministic uncertainty for terrestrial laser scanning observations based on intervals. *Journal of Applied Geodesy*, 19(3):385–394, 2025b. doi: doi:10.1515/jag-2025-0034.

NEUMANN, I & KUTTERER, H. Geodetic deformation analysis with respect to observation imprecision. In *Proceedings of the XXIII FIG Congress: Shaping the Change*, pages 1–15, Munich, Germany, 2006. TS 68 – Deformation Measurements of Dams (October 8–13, 2006).

NEUMANN, I & KUTTERER, H. Congruence tests and outlier detection in deformation analysis with respect to observation imprecision. *Journal of Applied Geodesy*, 1:1–7, 2007. doi: 10.1515/JAG.2007.001.